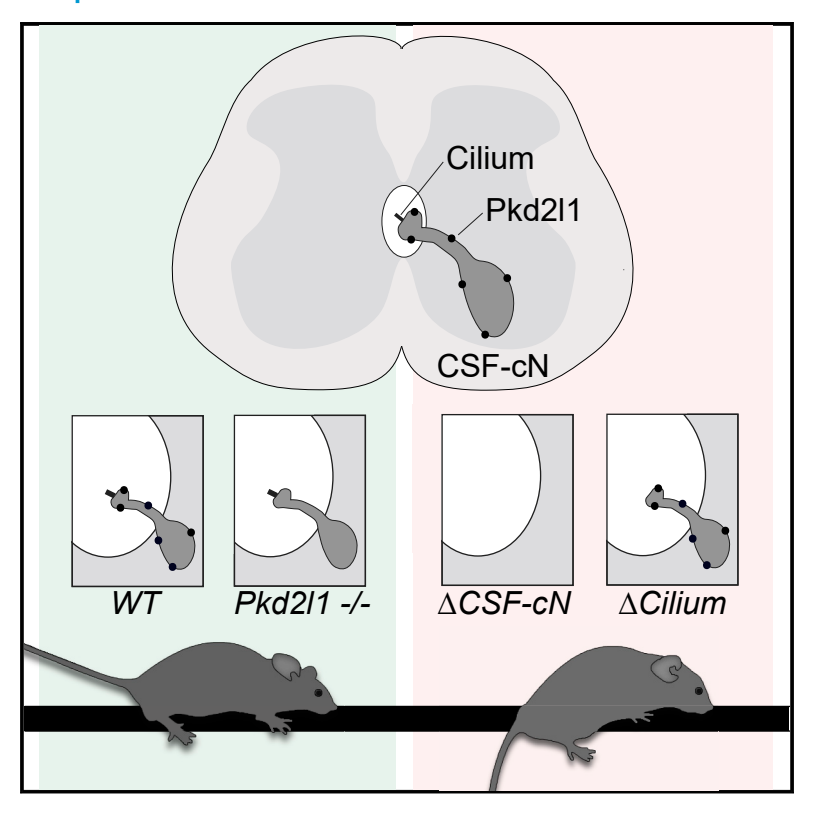
The role of intraspinal sensory neurons in the control of quadrupedal locomotion

Graphical abstract



Authors

Katrin Gerstmann, Nina Jurčić, Edith Blasco, Severine Kunz, Felipe de Almeida Sassi, Nicolas Wanaverbecq, Niccolò Zampieri

Correspondence

niccolo.zampieri@mdc-berlin.de

In brief

Cerebrospinal fluid-contacting neurons (CSF-cN) represent an evolutionary conserved vertebrate interoceptive system relaying sensory information from the CSF to spinal motor circuits. This study reveals CSF-cN's role in mammalian motor control where they contribute to orchestrate the precise execution of movements required for skilled locomotion.

Highlights

- CSF-cN are evolutionary conserved components of mouse spinal sensorimotor circuits
- Elimination of CSF-cN compromises adaptive motor control
- The cilium is required for CSF-cN function
- Pkd2l1 is dispensable for CSF-cN function in mice









Article

The role of intraspinal sensory neurons in the control of quadrupedal locomotion

Katrin Gerstmann,¹ Nina Jurčić,² Edith Blasco,² Severine Kunz,³ Felipe de Almeida Sassi,¹ Nicolas Wanaverbecq,^{2,5} and Niccolò Zampieri^{1,4,6,*}

¹Max Delbrück Center for Molecular Medicine, Robert-Rössle-Str. 10, 13125 Berlin, Germany

²Institut de Neurosciences de la Timone, Aix-Marseille Université (AMU) & CNRS, UMR7289, Timone Campus, 27 Boulevard Jean Moulin, 13005 Marseille. France

³Technology Platform for Electron Microscopy, Max Delbrück Center for Molecular Medicine, Robert-Rössle-Str. 10, 13125 Berlin, Germany

⁴Twitter: @ZampieriNiccolo ⁵Twitter: @N_Wanaverbecq

⁶Lead contact

*Correspondence: niccolo.zampieri@mdc-berlin.de https://doi.org/10.1016/j.cub.2022.04.019

SUMMARY

From swimming to walking and flying, animals have evolved specific locomotor strategies to thrive in different habitats. All types of locomotion depend on the integration of motor commands and sensory information to generate precisely coordinated movements. Cerebrospinal-fluid-contacting neurons (CSF-cN) constitute a vertebrate sensory system that monitors CSF composition and flow. In fish, CSF-cN modulate swimming activity in response to changes in pH and bending of the spinal cord; however, their role in mammals remains unknown. We used mouse genetics to study their function in quadrupedal locomotion. We found that CSF-cN are directly integrated into spinal motor circuits. The perturbation of CSF-cN function does not affect general motor activity nor the generation of locomotor rhythm and pattern but results in specific defects in skilled movements. These results identify a role for mouse CSF-cN in adaptive motor control and indicate that this sensory system evolved a novel function to accommodate the biomechanical requirements of limb-based locomotion.

INTRODUCTION

Animals have developed a wide variety of locomotor strategies to adapt to their environment. The ability to precisely control movements is essential for each mode of locomotion and depends on the dynamic integration of motor commands and sensory information. Planning and initiation of motor programs take place in the brain, whereas their execution is directed by the spinal cord. Spinal circuits combine descending input with sensory feedback in order to generate coordinated movements and reflexive actions. ^{1–3} Although the contributions of the somatosensory system have been extensively studied, the role of different sources of sensory information is less clear.

Cerebrospinal fluid-contacting neurons (CSF-cN) have been first described a century ago as sensory neurons lining the central canal in vertebrates. ^{4,5} They exhibit a peculiar morphology including a ciliated protrusion extending into the lumen of the central canal. ⁶ Thus, they have been thought to represent a sensory system monitoring CSF composition and flow. CSF-cN are inhibitory neurons and express ion channels known to be involved in sensory transduction, such as P2X and Pkd2l1. ^{7,8} The latter represents a specific marker of CSF-cN. ⁹ In larval zebrafish, CSF-cN are directly connected to primary motor neurons and V0v interneurons, glutamatergic premotor neurons that are part of the swimming central pattern generator. ^{10,11} Optogenetic stimulation of CSF-cN in resting larvae elicits low frequency

movements, whereas activation during active swimming results in inhibition of locomotion, thus indicating that CSF-cN differentially modulate motor activity depending on the state of the animal.¹⁰

In fish, CSF-cN sense changes in pH and spinal curvature. ^{12–14} In particular, calcium-imaging experiments revealed responses to both active and passive bending of the body axis, highlighting CSF-cN function as a mechanosensory system detecting the curvature of the spinal cord, either self-generated or induced by external forces. ^{11,12} Pkd2l1 has been shown to be crucial for CSF-cN mechanosensory function; in its absence, CSF-cN are not activated by spinal bending and behavioral responses are impaired. ^{12,15} Altogether these studies indicate that in fish, CSF-cN are the key component of a chemo- and mechanoreceptive sensory system that relay information about CSF composition and curvature of the body axis in order to modulate locomotor activity and control posture. ¹⁶

The biomechanical requirements and circuit mechanisms controlling wave-like propagation of swimming movements in fish versus on-ground locomotion in limbed vertebrates are substantially different, raising questions regarding the physiological function of CSF-cN.¹⁷ In this study, we analyzed CSF-cN connectivity and function in mice. We found that CSF-cN are directly integrated in spinal motor circuits and form ascending recurrent connections. Ablation of CSF-cN did not affect motor activity nor the generation of stereotyped locomotor patterns, such as



Article



walking and swimming, but resulted in selective defects in skilled locomotion. We observed an increase of foot slips and falls at the balance beam and the horizontal ladder, indicating that elimination of CSF-cN leads to defects in adaptive motor control. Surprisingly, we found that in mice, Pkd2l1 activity is dispensable for CSF-cN function. However, elimination of CSF-cN cilium is sufficient to completely recapitulate the phenotypes observed after neuronal ablation, thus demonstrating that this structure is necessary for sensory transduction. These findings indicate that during the evolutionary transition from swimming to walking, CSF-cN have acquired a novel role in order to adapt to the specific needs of limbed-based locomotion and are an essential part of the sensory feedback mechanisms that contribute to adaptive motor control required for skilled locomotion.

RESULTS

CSF-cN connect to key components of spinal motor circuits

We studied the physiological role of CSF-cN in the mammalian nervous system by obtaining genetic access using the *Pkd2l1::Cre* mouse line.¹⁸ We verified targeting specificity by lineage tracing with a nuclear GFP reporter line¹⁹ (*RosaΦHTB*) and found that at all spinal levels ~84% of labeled cells were Pkd2l1⁺ and presented the characteristic position and morphology of CSF-cN (Figures S1A and S1B). In addition, we did not observe reporter expression in any other cell type in the central nervous system (Figure S1C).

In order to explore CSF-cN connectivity, we first investigated synaptic targets by labeling presynaptic boutons with tdTomatotagged synaptophysin²⁰ (Ai34). We observed dense signal localized around the central canal and in the ventromedial part of the spinal cord at all axial levels (Figure 1A). Interestingly, key components of spinal motor circuits are characterized by stereotyped positioning in these areas along the entire rostrocaudal extent of the spinal cord. Median motor column (MMC) neurons controlling the activity of epaxial muscles are found in ventromedial location, whereas V0c neurons, cholinergic premotor interneurons, are positioned in the intermediate spinal cord in proximity to the central canal. 21,22 Thus, we asked whether MMC and V0c neurons receive synaptic input from CSF-cN. To test this hypothesis, we relied on the cholinergic nature and stereotyped position of these cell types to identify them (Figure 1B). We found putative synaptic contacts on $\sim 57\%$ of V0c and \sim 35% of MMC neurons at all spinal levels, as well as few instances of tdTomato+ boutons juxtaposed to lateral motor column (LMC) neurons at lumbar and cervical levels (~13%; Figures 1C and S1D). In addition, we investigated whether other cardinal ventral interneuron subtypes represent possible synaptic targets of CSF-cN. We found synaptic boutons in close proximity of Lhx1⁺ (V0/dI4)²³ and Chx10⁺ (V2a)²⁴ interneurons, but not onto calbindin⁺ (Renshaw cells)²⁵ and FoxP2⁺ (V1) ventral horn interneurons²⁶ (Figure 1D). Altogether, these data show that CSF-cN presynaptic terminals are found juxtaposed to key components of spinal motor circuits.

To confirm the anatomical findings and assess functional connectivity, we expressed channelrhodopsin-2²⁷ (ChR2, *Ai32*) in CSF-cN and used whole-cell patch-clamp recording combined to ChR2-assisted circuit mapping ²⁸ (CRACM) to identify

putative CSF-cN postsynaptic partners. First, to validate the optogenetic model in CSF-cN, we carried out a set of tests, and our data show that in voltage clamp mode ($V_p = 90 \text{ mV}$), reliable photocurrents with the characteristic properties-current with an initial transient and subsequent persistent phase-can be elicited in CSF-cN with a light pulse power set at 2 mW.mm⁻² (-150 and -65 pA for peak and steady state currents, respectively) with little changes in amplitude for further increase in power (Figures S2A and S2B; n = 12-16). Thus, to ensure reliable ChR2 activation, we used a power set at 5 mW.mm⁻². The analysis of the photocurrent current-voltage relationship (V_h -70 mV and $V_{\textit{Step}}$ from -90 to -10 mV, 20 mV increments) indicates that the current amplitude follows a linear regression with a current reversion at -10 mV (Figure S2C; n = 67). Further, we show that the photocurrents elicited with either repetitive light pulses (Figure S2D; n = 8) or with pulses of increased duration (Figure S2E; n = 11) remained stable. Finally, we compared the action potential (AP) discharge pattern induced in the same CSF-cN (current clamp mode at resting membrane potential, abbreviated asRMP) either following positive direct current (DC) injection (+20 pA) or exposure to light pulses of increasing duration and show that both stimuli triggered comparable spiking and AP discharge frequency (Figure S2F; n = 7) and that repetitive short light pulses reliably induced spiking over time (Figure S2G). Taken together, these data indicate that optical stimulation reliably generated ChR2 photocurrents and evoked AP discharge in ChR2+ CSF-cN.

Next, we assessed the functional connectivity between CSFcN and spinal interneurons. We recorded interneurons located close to the central canal (50 \pm 5 μ m; n = 20. Figure 2C) in the proximity of ChR2+ varicosities and determined their intrinsic electrophysiological, firing, and morphological properties (Figure 2A). The majority of the recorded interneurons (15/20) presented electrophysiological (r_m: 541 \pm 7 M Ω ; c_m: 26 \pm 2 pF), AP (AP half width: 2.0 ± 0.2 ms; discharge frequency: 26 ± 2 Hz, +50 pA DC current injection) and morphological properties compatible with V0c neurons identity²² (Figures 2B and 2C). The remaining cells (5/20) were characterized by a different physiological profile, suggesting that at least another interneuron subtype residing next to the central canal receive direct input from CSF-cN (data not shown). In line with the neurotrasmitter phenotype of CSF-cN, we found that short light pulses evoked inward inhibitory responses in these neurons (V_h -70 mV and E_{Cl} -60 mV; 20/500 neurons patched) that were completely abolished in the presence of gabazine (Figures 2D and 2E; n = 20). Thus, physiological analysis confirms functional connectivity between CSF-cN and spinal interneurons positioned around the central canal.

CSF-cN are reciprocally connected and receive sparse input from spinal interneurons

Next, we explored sources of presynaptic input to CSF-cN by using rabies virus (RV) retrograde monosynaptic tracing. ²⁹ We selectively targeted CSF-cN for rabies infection and transsynaptic spread by injecting a mixture of Cre-dependent helper adenoassociated viruses (AAVs) at lumbar (L) level 1 of *Pkd2l1::Cre* mice (AAV-syn-FLEX-splitTVA-EGFP-tTA and AAV-TREtight-mTagBFP2-B19G³⁰). Three weeks later, EnvA pseudotyped G-deficient RV (RVΔG-mCherry/EnvA) was delivered at the



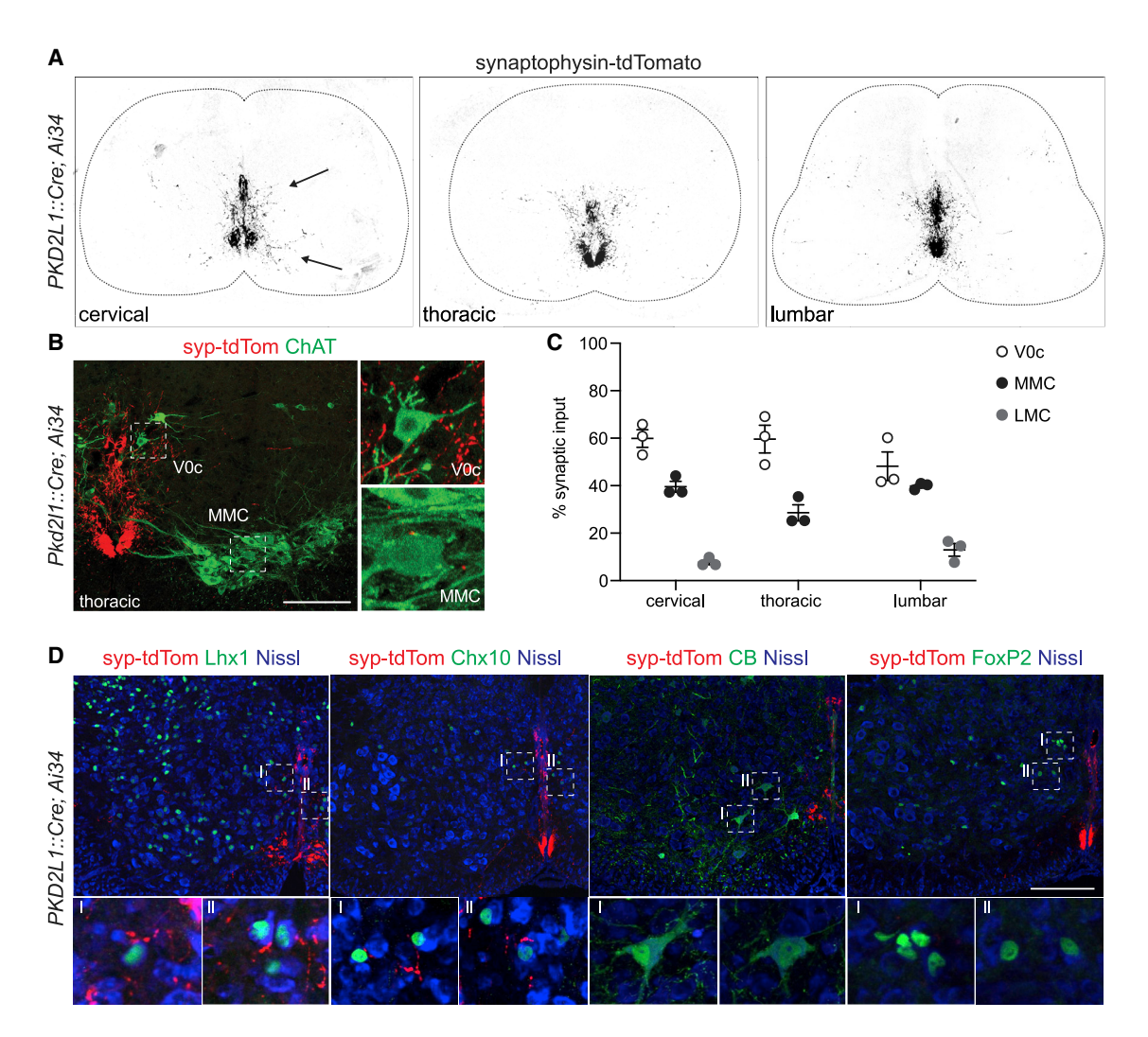


Figure 1. CSF-cN project to key components of spinal motor circuits

(A) Representative images of synaptophysin-tdTomato labeling of CSF-cN at cervical, thoracic, and lumbar levels of P7 Pkd2l1::Cre; Ai34 mice. Arrows point to dense labeling nearby the central canal and the ventromedial area of the spinal cord.

- (B) Representative images of synaptophysin-tdTomato puncta in close contact with ChAT⁺ V0c and MMC neurons at the thoracic level of P7 *Pkd2l1::Cre; Ai34* mice. Scale bar, 200 μm. Magnifications show single z-planes.
- (C) Proportion of V0c, MMC, and LMC neurons that receive synaptic input from CSF-cN at cervical, thoracic, and lumbar levels (n = 3).
- (D) Representative images of synaptophysin-tdTomato puncta in close contact with ventral interneurons subtypes. We found Tomato⁺ puncta on Lhx1⁺ (V0/dl4) and Chx10⁺ (V2a) interneurons, but not onto calbindin⁺ (CB) ventral horn interneurons (Renshaw cells) and FoxP2⁺ (V1) interneurons. Scale bar, 200 μm. Magnifications show single z-planes.

See also Figure S1 and Video S5.

same level (Figure 3A). We first examined starter cells, defined as neurons infected by both AAV and RV and found BFP+; RV+ neurons around the central canal at the point of injection, with morphologies and positions characteristic of CSF-cN (Figures 3B–3D). We next focused on transynaptically labeled neurons and found that the majority of BFP-; RV+ cells were also CSF-cN (~85%) but mainly located at more caudal levels of the spinal cord, thus indicating that CSF-cN are reciprocally connected, with caudal neurons sending input to rostral segments (Figures 3D and S3A–S3C). To further investigate whether CSF-cN make ascending axonal projections, as suggested by rabies tracing experiments and previously shown in zebrafish, 31 we drove expression of the avian tumor virus receptor A (TVA) in

CSF-cN at L1 by focal injection of AAV-FLEX-TVAmCherry in Pkd2l1::Cre mice and then probed the directionality of CSF-cN axons by delivering RV Δ G-GFP/EnvA, either at rostral (T10) or caudal (L3) levels (Figures 3F and 3G). We observed retrograde infection of TVA expressing CSF-cN only after rabies injection at T10, thus indicating that CSF-cN send axons only to more rostral segmental levels (Figures 3F and 3G). Finally, we assessed whether CSF-cN form functional reciprocal synaptic contact. By using CRACM, CSF-cN were recorded in voltage clamp mode (V_h 0 mV) at the ChR2 current reversal potential to avoid recording contamination with the photocurrent (Figures 3H and S2C). We show that exposure to short light pulses evoked synaptic responses in all recorded CSF-cN



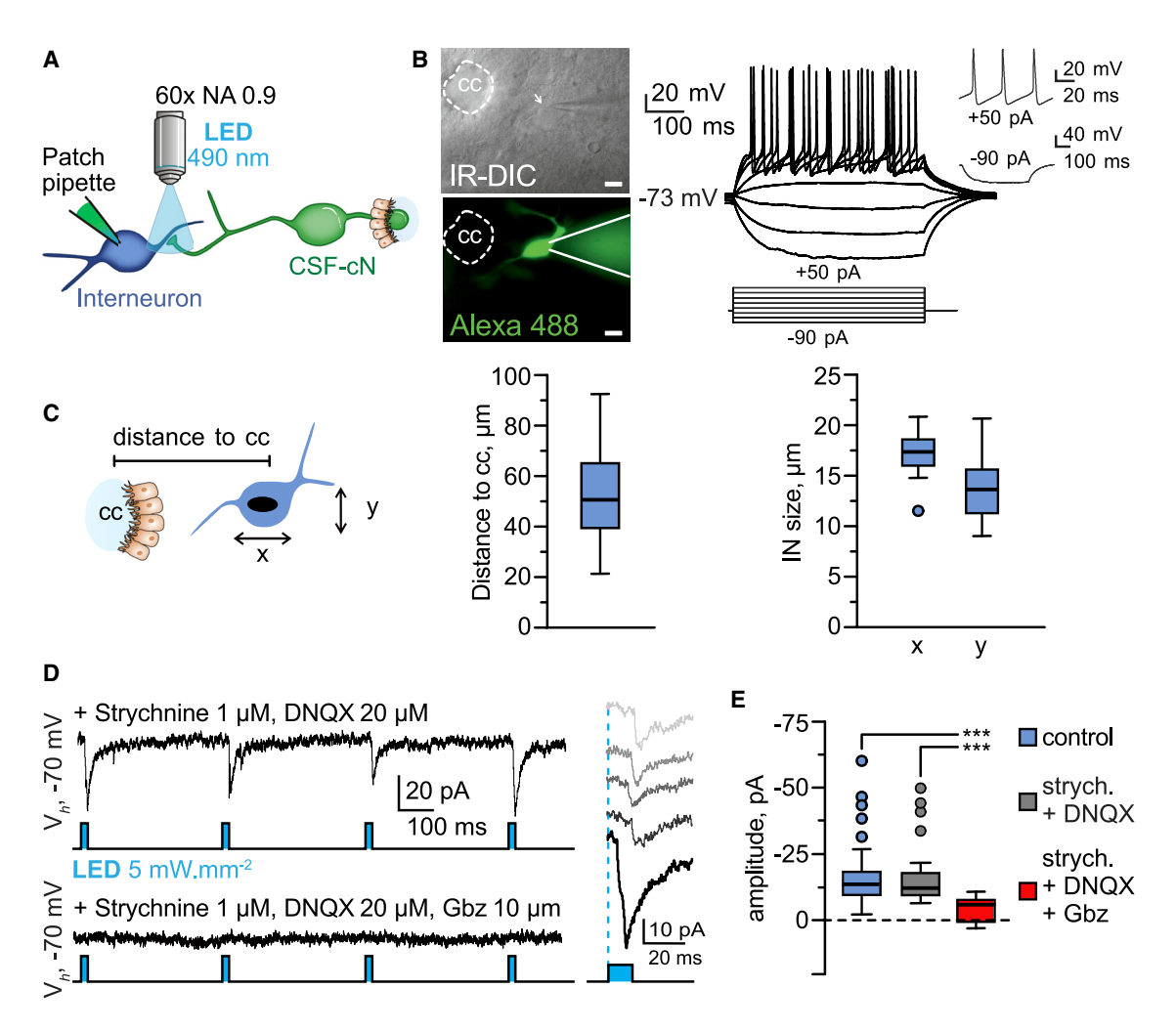


Figure 2. CSF-cN form functional synaptic contact with spinal interneurons

(A) Schematic of patch-clamp recordings and ChR2-assisted circuit mapping to identify putative CSF-cN postsynaptic partners.

(B) Micrographs showing a responsive interneuron position (arrow, IR-DIC) and its morphology (green, Alexa488 dialysis during recording, scale bars, 20 μm). Right, traces showing the electrophysiological properties of the interneurons shown on the left. Recording in current clamp at RMP –73 mV and injection of DC current steps from –90 to +50 pA (increments: +20 pA) showing a large hyperpolarization and sustained high frequency AP discharge upon negative and positive direct current injection, respectively.

(C) Schematic (left) illustrating parameters used for quantifying the position (center) and size (right) of responsive neurons (n = 20; mean ± SD).

(D) Representative traces of the photoevoked inward currents recorded in one interneuron (voltage clamp mode, V_h –70 mV and E_{Cl} –60 mV) upon repetitive optical activation (10 ms, 5 mW.mm⁻² every 500 ms, see LED pulse under the traces) of ChR2⁺ CSF-cN terminals present on the neuron. Top: recording in the presence of 1 μ M strychnine and 20 μ M 6,7-dinitroquinoxaline-2,3-dione (DNQX), bottom: addition to the bath of 10 μ M gabazine (Gbz) completely blocks the evoked responses. Traces are the average of 5 consecutive recordings and the inset on the right show individual responses for the first light pulse.

(E) Summary box-whisker plot for IPSC current amplitude in control (blue box, CTR), in the presence of strychnine and DNQX alone (gray box, SD), and with gabazine added to the bath (red box, SDG). (Kruskal Wallis test: $\chi^2 = 62,589$, df = 2, p = 2.564 × 10⁻¹⁴; post-hoc Wilcoxon pairwise test: CTR versus SD, p = 0.32; CTR and SD versus SDG, p = 1.3 × 10⁻¹³ and p = 2×10⁻⁶, respectively; n = 20). See also Figure S2.

(19/19). Moreover, these synaptic currents were outward and completely abolished in the presence of gabazine and picrotoxin (Figures 3I and 3J; n = 19), as expected for the chloride equilibrium potential (E_{Cl}) set at -60 mV and the activation of GABA_A receptors.

The remaining presynaptic input consisted of sparse labeling of spinal interneurons without any distinct positional organization (Figures 3C–3E). We analyzed the neurotransmitter phenotype of CSF-cN presynaptic partners by assessing expressions of *VGAT* and *VGLUT2* and found that the majority of

presynaptic neurons were $VGAT^+$, including CSF-cN that are known to have GABAergic phenotype³² (Figures S3D and S3E). Altogether, these data indicates that CSF-cN are reciprocally connected and receive sparse input mainly by local inhibitory interneurons.

CSF-cN are required for skilled locomotion

Next, to study the function of CSF-cN in motor control, we crossed the *Pkd2l1::Cre* line with the *RosaΦDTR* allele to drive expression of the diphtheria toxin receptor³³ (DTR). Diphtheria



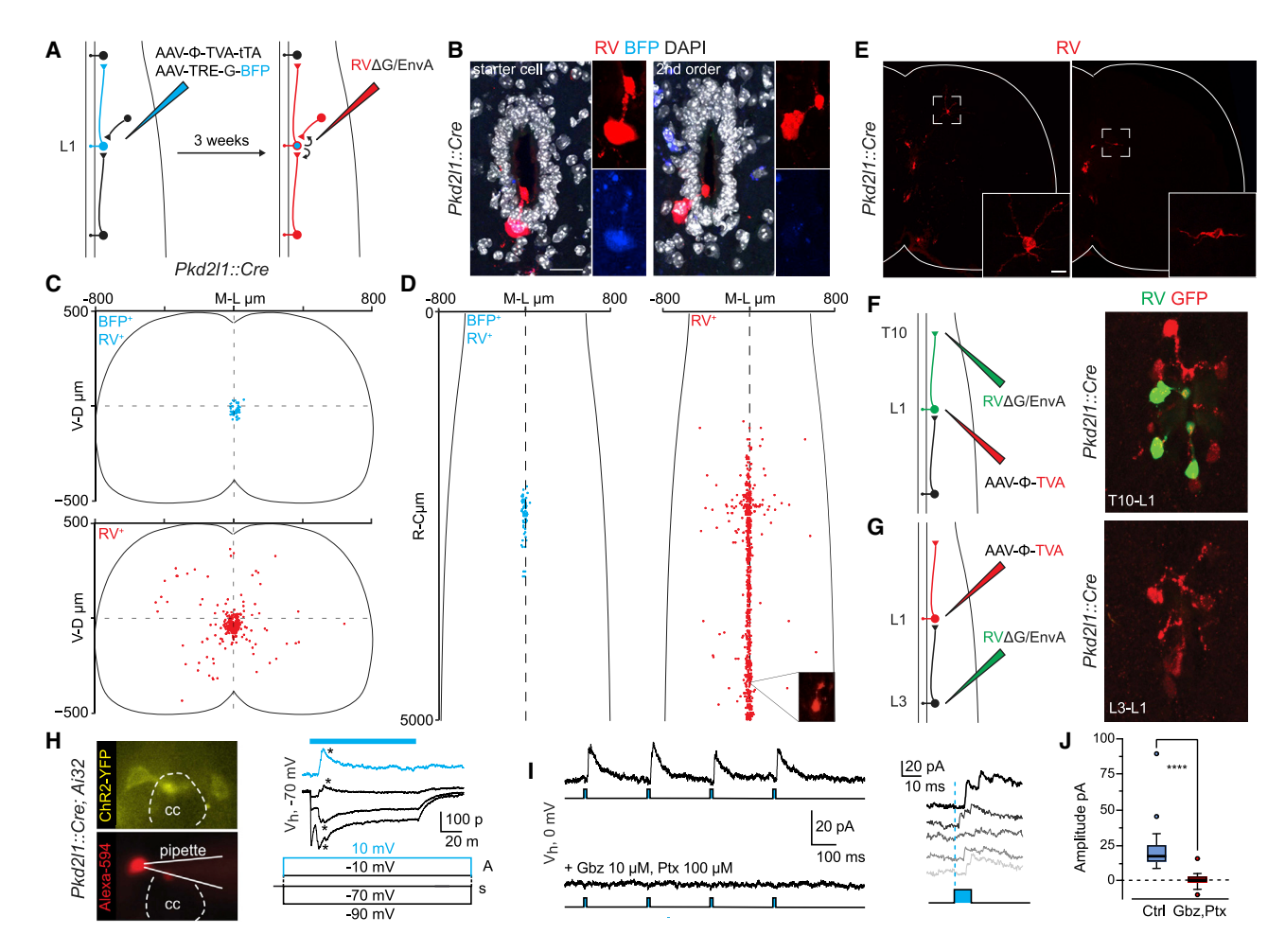


Figure 3. CSF-cN are reciprocally connected and receive sparse input from local spinal interneurons

- (A) Schematic illustrating rabies monosynaptic tracing approach to identify cells providing input to CSF-cN. A mix of Cre-dependent helper AAVs driving the expression of TVA and G was injected at L1 of P7 *Pkd2l1::Cre* mice. However, 3 weeks later, RVΔG-mCherry/EnvA was injected at the same position, and after 7 days spinal cords were examined.
- (B) Representative images of BFP $^+$; RV $^+$ starter cells and BFP $^-$; RV $^+$ second order CSF-cN. Scale bars, 20 μm .
- (C and D) Digital reconstruction of medio-lateral/dorso-ventral position (C) and medio-lateral/rostro-caudal position (D, thoracic segment on top) of starter cells (blue) and second order cells (red); n = 3.
- (E) Representative images of second order neurons labeled in rabies tracing experiments from CSF-cN.
- (F) Schematic illustration of retrograde tracing approach to test directionality of CSF-cN axonal projections. Injection of AAV-FLEX-TVAmCherry in *Pkd2l1::Cre* mice at P7 was followed 3 weeks after by RVΔG-GFP/EnvA injection at T10. Representative image shows AAV⁺/RV⁻ and AAV⁺/RV⁺ cells at L1.
- (G) Schematic illustration of retrograde tracing approach to test directionality of CSF-cN axonal projections. Injection of AAV-FLEX-TVAmCherry in *Pkd2l1::Cre* mice at P7 was followed 3 weeks by RVΔG-GFP/EnvA injection at L3. Representative image shows AAV⁺/RV⁻ cells at L1, no RV⁺ cells were detected.
- (H) Representative epifluorescence image of one ChR2 $^+$ CSF-cN recorded in an acute lumbar spinal cord slice (250 μ m, cc, central canal) obtained from a *Pkd2l1::Cre; Rosa\PhiChrR2* mice showing ChR2 expression through YFP (top) and Alexa 594 fluorescence (bottom) upon cell dialysis through the patch pipette. Right, voltage-dependance of the ChR2 photoevoked currents in CSF-cN recorded in voltage clamp mode (V_n –70 mV) at the voltage potential steps indicated under the traces. Note the decrease in the photocurrent amplitude with depolarizing voltage steps (null for –10 mV, see also Figure S2C) and the presence of currents (*) that develop shortly after the onset of the photocurrent and are either inward or outward for potentials more hyperpolarized or depolarized than –60 mV (E_{Cl}), respectively.
- (l) Representative traces of the photoevoked outward currents recorded in one CSF-cN (voltage clamp mode, V_h 0 mV and E_{Cl} –60 mV) upon repetitive optical activation (10 ms, 5 mW.mm⁻² every 500 ms, see LED pulse under the traces) of ChR2+ CSF-cN terminals present on the neuron. Top: control condition. Bottom: 100 μ M picrotoxin (Ptx) and 10 μ M gabazine (Gbz) blocked the evoked responses. The traces illustrated are the average of 5 consecutive recordings and the inset on the right shows for the first light pulse individual responses.
- (J) Summary box-whisker plot for IPSC current amplitude in control (CTR) and in the presence Gbz and Ptx (Wilcoxon signed rank test: p = 0.00013; n = 19). See also Figure S3.

toxin (DT) administration in adult mice resulted in the elimination of >80% CSF-cN within 2 weeks (Figures 4A, 4B, S4A, and S4B). We first evaluated the effect of acute ablation of CSF-cN on

general locomotor function associated with exploratory behavior by using the open field test. We did not find any significant difference between DT- and PBS-treated mice in activity, speed,

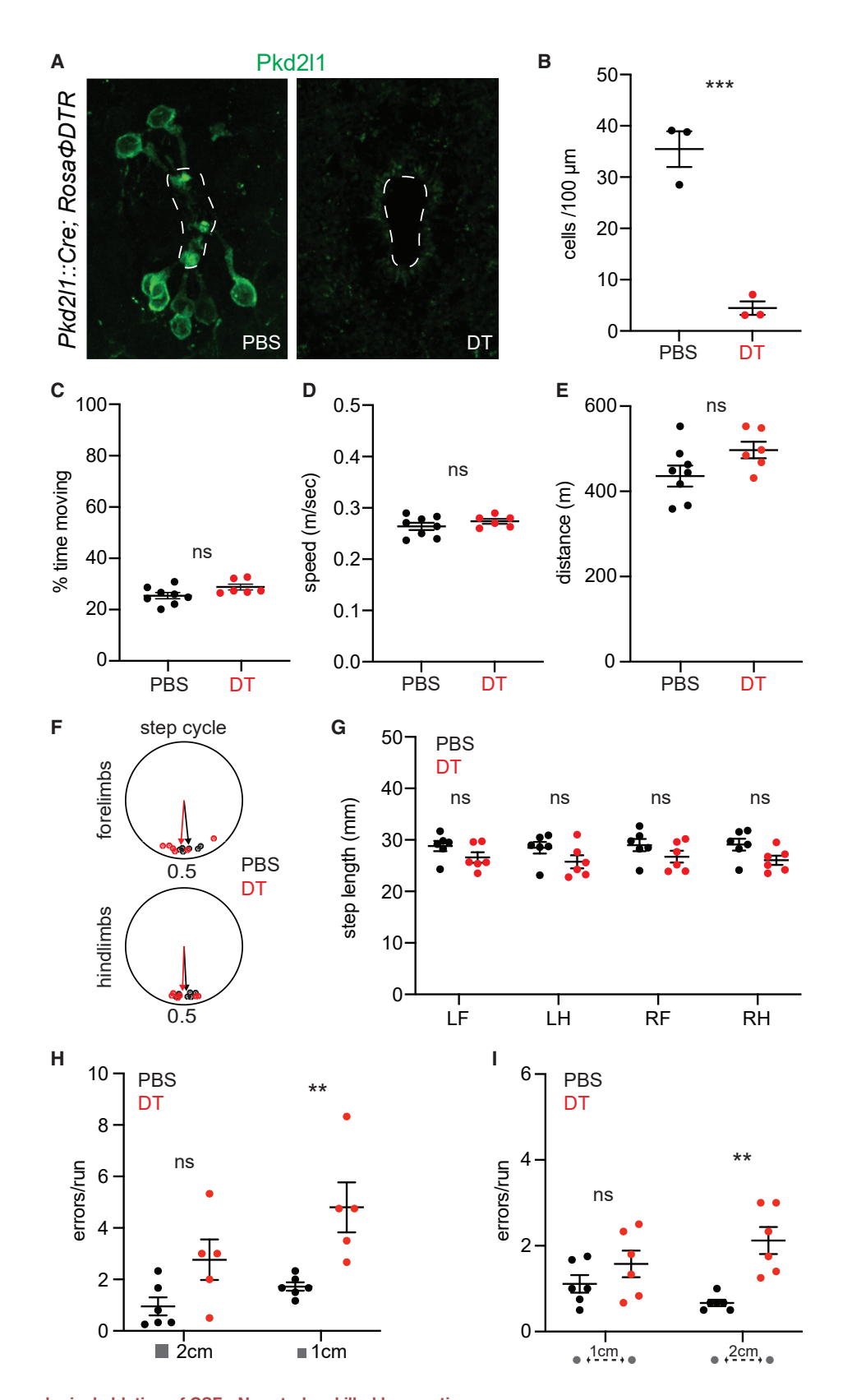


Figure 4. Pharmacological ablation of CSF-cN perturbs skilled locomotion

(A) Representative images of Pkd2l1⁺ neurons around the central canal 60 days after PBS (left) or DT (right) injection in *Pkd2l1::Cre; RosaΦDTR* mice.

(B) Quantification of Pkdl21⁺ neurons around the central canal 60 days after PBS (n = 3) or DT (n = 3) injection in *Pkd2l1::Cre; RosaΦDTR* mice.





distance traveled, and turning behavior (Figures 4C-4E and S4G). Next, we performed kinematic analysis on freely walking mice to evaluate gait and did not observe any effect on step cycle, step length, base of support, body stability, and the precision of foot placement, key parameters describing limb movement and coordination during unperturbed locomotion³⁴ (Figures 4F, 4G, S4C, S4H, and S5; Video S1). These data show that elimination of CSF-cN does not affect activity or generation of the patterns and rhythms of muscle contraction necessary for walking gait in mice. In larval zebrafish, CSF-cN have been shown to have an important role for postural control. 11 Thus, we evaluated tasks requiring control of trunk position and stability. First, we scored spontaneous rearing events and found no effect of CSF-cN ablation on rearing duration and frequency (Figure S4D; data not shown). Second, we tested swimming, a locomotor behavior that requires coordination of limbs and trunk in order to obtain directional movements.35 We did not observe any difference in speed or in the angle between the trunk and the water line, an indicator of postural control³⁶ (Figures S4E and S4F; Video S2). These experiments show that elimination of CSF-cN does not perturb postural control.

Finally, we tested skilled locomotion by assessing performance at the balance beam and horizontal ladder, tasks that are known to require precise sensory feedback in order to achieve accuracy in foot placement.³⁷ We used beams and ladders of different widths and rung spacing in order to assess the effect of progressively more difficult conditions.¹ In both tasks, DT-treated mice presented clear deficits in motor performance (Videos S3 and S4) that resulted in an increase in the numbers of foot slips and falls, which was significantly higher than control animals in the more challenging configurations (Figures 4H and 4I). Thus, these data indicate that CSF-cN are required for skilled locomotion.

The cilium is necessary for CSF-cN function

Next, we wondered whether the Pkd2l1 channel is necessary for CSF-cN function in mice, as in zebrafish, its elimination impairs mechanosensation and behavioral responses to changes in spinal bending. ^{12,15} To address this question, we analyzed locomotor behavior in Pkd2l1 knockout mice³⁸ (*Pkd2l1*^{-/-}; Figure 5A). In line with the results obtained after neuronal ablation experiments, these mice did not show any phenotype at the open field, gait analysis, and swimming tests (Figures 5B–5D and S5; data not shown; Videos S1 and S2). Surprisingly, *Pkd2l1*^{-/-} mice performance at the balance beam and horizontal ladder was also indistinguishable from control mice (Figures 5E and 5F; Videos S3 and S4). Altogether, these data suggests that CSF-cN function in mice does not require Pkd2l1 activity.

Cilia have been known to function as a mechanosensory organelle responding to fluid flow in many different cell types and most notably in sensory neurons. The intraflagellar transporter 88 (Ift88) is part of the Ift-B complex that is crucial for transport of ciliary proteins and its elimination suppress ciliogenesis.³⁹ Thus, to study the consequences of preventing cilium formation in CSF-cN, we crossed the Pkd2/1::Cre allele with the conditional Ift88^{fl} mouse line⁴⁰ (Pkd2I1::Cre^{+/-}; Ift88^{fl/fl}, hereafter referred to as $\Delta Cilia$). We first confirmed success of this strategy by visualizing CSF-cN protrusions in the central canal and the associated cilium. In control animals, we found that >70% of Pkd2l1⁺ apical processes presented a cilium, whereas in △Cilia mice, we found a significant reduction in the occurrence of ciliated CSF-cN (~35%; Figures 6A and 6B). Moreover, electron microscopy analysis confirmed that conditional elimination of Ift88 prevents ciliogenesis in CSF-cN (Figure 6C). Next, we evaluated locomotor behavior in $\Delta Cilia$ mice. We did not observe any significant defect in the open field, gait analysis, and swimming tests (Figures 6D-6G, S5, and S6; Videos S1 and S2). In contrast, the performance of $\Delta Cilia$ mice at the balance beam and horizontal ladder was perturbed (Videos S3 and S4). Strikingly, quantification of foot slips and foot falls revealed that △Cilia made significantly more mistakes when walking on the more challenging versions of the tests, thus precisely recapitulating the phenotype observed after CSF-cN ablation (Figures 6H and 6I). Altogether, these data show that the behavioral defects observed after elimination of the cilium phenocopy the ones occurring after neuronal ablation, thus indicating that this structure is necessary for CSFcN function in motor control in mice.

DISCUSSION

In this study, we investigated the physiological role of CSF-cN, an evolutionary conserved vertebrate sensory system, in limbed mammals. We found that these neurons are integrated into spinal motor circuits and contribute to adaptive motor control necessary for skilled locomotion. CSF-cN function in mice does not require the activity of the Pkd2l1 channel but entirely depends on its cilium, thus pointing to a key role for this mechanosensory structure in monitoring CSF flow. Altogether, our data suggest a model where CSF-cN provide an additional source of proprioceptive information by monitoring spinal curvature and represent an integral component of the sensory feedback mechanisms necessary for adaptive motor control.

Kolmer and Agduhr first described a peculiar population of sensory neurons lining the central canal and proposed that they constitute a sensory organ relaying information from the

⁽C–E) Locomotor activity during a 90 min open field test. Percentage of time spent moving (C), speed (D) and distance traveled (E) in adult $Pkd2l1::Cre; Rosa\Phi DTR$ mice 14 days after PBS (n = 8) or DT (n = 6) treatment.

⁽F) Step cycle in adult $Pkd2/1::Cre; Rosa\Phi DTR$ mice 14 days after PBS (n = 6) or DT (n = 6) treatment.

⁽G) Step length in adult Pkd2l1::Cre; RosaФDTR mice 14 days after PBS (n = 6) or DT (n = 6) treatment (LF, left forelimb; LH, left hindlimb; RF, right forelimb; RH, right hindlimb).

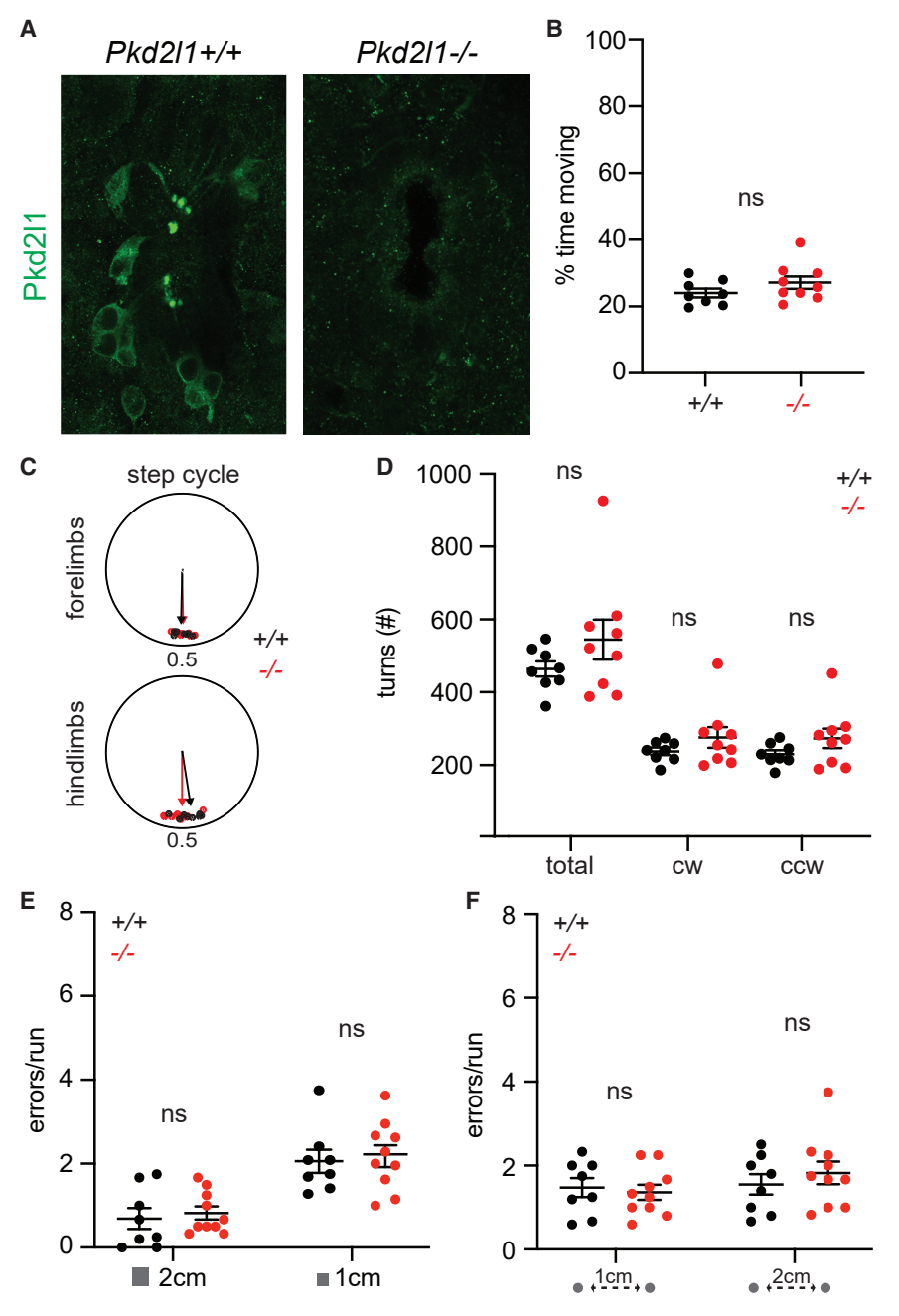
⁽H) Quantification of foot placement errors (slips and falls) in the balance beam test with 2 cm (left) or 1 cm (right) beam width in adult *Pkd2l1::Cre; RosaΦDTR* mice 14 days after PBS (n = 6) or DT-injection (n = 5).

⁽I) Quantifications of foot placement errors (slips and falls) in the horizontal ladder test with 1 cm (left) or 2 cm (right) rung distance in adult $Pkd2I1::Cre; Rosa\Phi DTR$ mice 14 days after PBS (n = 6) or DT-injection (n = 6).

Mean \pm SEM, paired t test, ns p > 0.05, ** p < 0.01, *** p < 0.001.

See also Figures S4 and S5 and Videos S1, S2, S3, and S4.





CSF.^{4,5} CSF-cN function has remained elusive until recent studies in lamprey and zebrafish revealed important roles in modulation of swimming and postural control.^{10,12,13} CSF-cN have been shown to provide information to the motor system about active and passive curvatures of the body axis by sensing fluid flow along the central canal.^{12,15,41} In fish, the importance of monitoring curvature along the rostro-caudal axis of the spinal cord is clear, as swimming relies on the rhythmic propagation of an undulatory pattern of muscle contraction. The introduction of limbs has led to the reorganization of motor circuits in order to accommodate the biomechanical requirements of terrestrial locomotion.¹⁷ The coordination of limb movements and precision of foot placement represent a critical feature of motor

Figure 5. Pkd2l1 elimination does not affect locomotion

- (A) Representative images of Pkd2l1 staining in adult $Pkd2l1^{+/+}$ and $Pkd2l1^{-/-}$ animals.
- (B) Percentage of moving time in adult $Pkd2l1^{+/+}$ (n = 8) and $Pkd2l1^{-/-}$ (n = 9) during 90 min open field test.
- (C) Step cycle of forelimbs (top) and hindlimbs (bottom) in adult $Pkd2l1^{+/+}$ (n = 8) and $Pkd2l1^{-/-}$ (n = 9).
- (D) Analysis of turning behavior (total, clockwise, and counterclockwise turns) during a 90 min open field test in adult *Pkd2l1*^{+/+} (n = 8) and *Pkd2l1*^{-/-} (n = 9) mice.
- (E) Quantification of foot placement errors (slips and falls) in the balance beam test with 2 cm (left) or 1 cm (right) beam width in adult $Pkd2l1^{+/+}$ (n = 8) and $Pkd2l1^{-/-}$ (n = 10).
- (F) Quantification of foot placement errors (slips and falls) in the horizontal ladder test with 1 cm (left) or 2 cm (right) rung distance in adult $Pkd2/11^{+/+}$ (n=8) and $Pkd2/11^{-/-}$ (n = 10).

Mean \pm SEM; paired t test, ns p > 0.05.

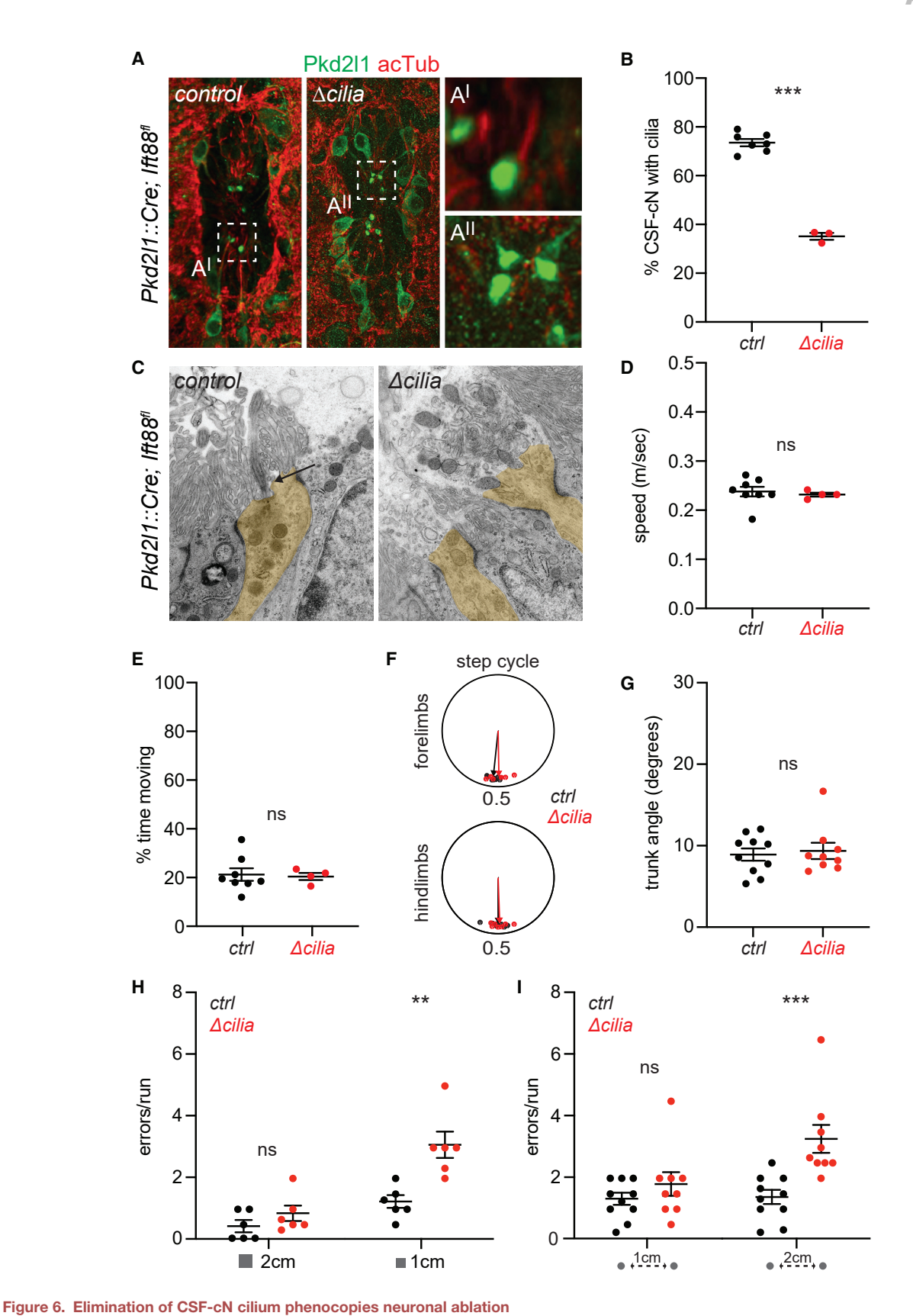
See also Figure S5 and Videos S1, S2, S3, and S4.

control in over ground locomotion.⁴² In particular, it is especially important for navigating the diverse terrains and obstacles animals are confronted with in the wild and require dynamic integration of different sources of sensory information.³⁷ In our experiments, we observed that locomotor patterns and rhythms, as well as the accuracy of foot placement, are not affected during unperturbed locomotion on a plexiglass runway. However, under more challenging conditions at the balance beam and horizontal ladder, where movements need to be more precisely controlled, we found a significant increase in the number of foot slips and falls. CSF-cN, by sensing spinal bending, can provide an extra layer of proprioceptive information that is dispensable during normal locomotion but required for skilled locomotion. Thus, a sensory system modulating wave-like movements at

the basis of swimming in fish may have evolved a novel role in the control of adaptive motor responses necessary to precisely regulate limb and body movements in limbed vertebrates.

At circuit level, we observed input-output connectivity patterns that are consistent with CSF-cN physiological role in sensorimotor integration. We found CSF-cN presynaptic puncta on motor neurons, thus possibly providing a direct way to regulate motor output, and on cardinal ventral interneuron subtypes such as ChAT+ V0c, Lhx1+ V0/dl4, and Chx10+ V2a interneurons, indicating connectivity to key components of spinal premotor circuits. At the physiological level, we confirmed that CSF-cN make functional inhibitory connections with spinal interneurons located around the central canal. However, we could not record





(A) Representative images of Pkd2l1+ CSF-cN apical protrusions and acetylated-tubulin+ cilia in adult control and Δcilia mice. High magnifications of Pkd2l1+ protrusion in the central canal of control (AI) and $\Delta cilia$ (AII) mice.

Article



functional connections to motor neurons. This discrepancy with the anatomical findings could be due to sparse connectivity and the technical limitation of finding intact connections in spinal cord coronal slices. In terms of input connectivity to CSF-cN, rabies monosynaptic tracing experiments revealed inputs from local spinal interneurons mostly of inhibitory character. Presynaptic inhibition could control the gain of CSF-cN activity, a well-known mechanism for tuning somatosensory feedback in spinal circuits. $^{\rm 43}$ In addition, we observed abundant recurrent connectivity between CSF-cN, with neurons located at caudal spinal segments sending ascending input to ones at more rostral levels. Zebrafish CSF-cN have been shown to form ascending axonal projections,44 and prominent bilateral CSF-cN axonal bundles can be found in the medial aspects of the ventral white matter in mice (Video S5). An inhibitory feedback loop from posterior to anterior CSF-cN is well suited for coordination of undulatory movements in fish, but its significance for limb-based locomotion remains to be explored.

At the behavioral level, our data show that in mice, elimination of CSF-cN does not perturb general motor activity and the generation of rhythmic patterns of limb movement necessary for the production of stereotyped locomotor actions, such as walking and swimming. In contrast, we observe an increase of foot slips and falls at the balance beam and horizontal ladder, indicating that the precision in motor control required for performing skilled movements is perturbed. Interestingly, the effect is significant only in the most challenging versions of the tasks. These data support the idea that multiple sources of sensory information, including cutaneous and muscle afferents, the visual, and the vestibular systems, are integrated to precisely adjust limb and body movements in order to prevent foot slippage during the execution of skilled actions and suggest that CSF-cN may provide proprioceptive information about body position. Previous work in lamprey and zebrafish, along with our observation that elimination of the cilium completely recapitulates the defects observed after neuronal ablation, point to a role for CSF-cN in mice as mechanoreceptive sensory neurons detecting curvature of the spinal cord by sensing CSF flow in the central canal.41 Thus, we propose that CSF-cN by monitoring spinal bending provide additional proprioceptive feedback informing the motor system on axial position that is used to adjust trunk and limb movement during locomotion. Walking on narrow paths or challenging terrains introduces forward and lateral displacements in the body axis that can be finely monitored by CSF-cN. For example, walking on a balance beam reduces lateral stability by decreasing the available base of support or walking on the horizontal ladder requires to overextend hindlimbs in order to land on the same rung where the forelimbs touched down, thus resulting in exaggerated hip torsion.³⁷

Surprisingly, we did not observe any defect in locomotor behavior upon elimination of Pkd2l1. This is in contrast with its requirement for CSF-cN function in zebrafish, thus raising interesting questions regarding additional molecular effectors in mammals. Our study does not exclude the possibility that in mice, Pkd2l1 might be selectively required for chemosensation, as this channel has been shown to respond directly to pH changes. The ability to monitor CSF composition has been proposed to be part of a homeostatic mechanisms common to all vertebrates for counteracting the effects of pH changes by reducing muscle activity. It will be interesting to address whether chemosensation in mammalian CSF-cN could serve as system for modulating motor behavior in response to changes in the internal state of the animal, for example, in case of fatigue or sickness.

Altogether, our anatomical and functional data indicate that CSF-cN are an important component of sensorimotor circuits in the mammalian spinal cord, contributing to adaptive motor control. This study opens the way for future work to address exciting questions on how information on CSF composition and flow is encoded by CSF-cN and integrated at a circuit level with other sensory inputs, such as muscle and cutaneous feedback, in order to orchestrate flawless execution of motor programs.

STAR*METHODS

Detailed methods are provided in the online version of this paper and include the following:

- KEY RESOURCES TABLE
- RESOURCE AVAILABILITY
 - Lead contact
 - Material availability
 - Data and code availability
- EXPERIMENTAL MODEL AND SUBJECT DETAILS
 - Animal Experimentation Ethical Approval
 - Animal models
- METHODS DETAILS
 - Ablation of CSF-cNs
 - Behavioral experiments
 - O Perfusion and tissue preparation
 - Slice preparation, electrophysiology and optogenetic stimulation

Mean \pm SEM; paired t test, ns p > 0.05, ** p<0.01, *** p < 0.001.

⁽B) Quantification of Pkd2l1+ CSF-cN apical protrusions bearing an acetylated-tubulin+ cilium in control and Δcilia mice (n = 3).

⁽C) Representative electron microscopy images of CSF-cN (highlighted in yellow) in control (left) and \(\Delta cilia \) (right) mice. Arrow point to the cilium.

⁽D) Average speed during a 90 min open field test in adult control (n = 8) and $\Delta cilia$ (n = 4) mice.

⁽E) Percentage of moving time in adult control (n = 7) and $\Delta cilia$ mice (n = 4) during 90 min open field test.

⁽F) Step cycle of forelimbs (top) and hindlimbs (bottom) in adult control (n = 10) and $\Delta cilia$ mice (n = 9).

⁽G) Quantification of trunk angle between body axis and water line during swimming task in adult control (n = 10) and Δcilia mice (n = 9).

⁽H) Quantification of foot placement errors (slips and falls) in the balance beam test with 2 cm (left) or 1 cm (right) beam width in adult *control* (n = 6) and Δ*cilia* mice (n = 6).

⁽I) Quantification of foot placement errors (slips and falls) in the horizontal ladder test with 1 cm (left) or 2 cm (right) rung distance in adult control (n = 10) and $\Delta cilia$ mice (n = 9).





- Immunohistochemistry
- Viral tracings
- O Fluorescent in situ hybridization
- Positional analysis
- Electron microscopy
- Tissue clearing and light-sheet microscopy
- QUANTIFICATION AND STATISTICAL ANALYSIS

SUPPLEMENTAL INFORMATION

Supplemental information can be found online at https://doi.org/10.1016/j.cub.2022.04.019.

ACKNOWLEDGMENTS

We thank Liana Kosizki for technical support and the MDC Advanced Light Microscope facility for assistance with image acquisition and analysis, Sofia Pimpinella for helping with spinal injections, and Pierre-Louis Ruffault for advice with experimental design. We thank Robert Manteufel, Ilka Duckert, and Florian Keim for animal care; Baptiste Lasbats and Lilly von Kalckreuth for assistance with behavioral experiments; Nikos Balaskas, Marco Beato, Joriene De Nooij, and members of the Zampieri and Wanaverbecq laboratories for insightful comments on the manuscript. N.Z. and N.W. were supported by a DFG-ANR international collaborative grant (MotAct-CSF. DFG ZA 885/1-2 and ANR-16-CE92-0043); N.W. by AMU and CNRS INSB.

AUTHOR CONTRIBUTIONS

Conceptualization, K.G., N.W., and N.Z.; investigation, K.G., N.J., E.B., S.K., and F.d.A.S.; formal analysis, K.G., N.J., E.B., and S.K.; writing – original draft, K.G. and N.Z.; writing – review and editing, K.G., N.W., and N.Z.; funding acquisition, N.W. and N.Z.; resources, N.W. and N.Z.; supervision, N.W. and N.Z.

DECLARATION OF INTERESTS

The authors declare no competing interests.

Received: October 12, 2021 Revised: March 4, 2022 Accepted: April 8, 2022 Published: May 4, 2022

REFERENCES

- Rossignol, S., Dubuc, R., and Gossard, J.-P. (2006). Dynamic sensorimotor interactions in locomotion. Physiol. Rev. 86, 89–154.
- Koch, S.C. (2019). Motor task-selective spinal sensorimotor interneurons in mammalian circuits. Curr. Opin. Physiol. 8, 129–135.
- 3. Tuthill, J.C., and Azim, E. (2018). Proprioception. Curr. Biol. 28, R194–R203
- Kolmer, W. (1921). Das "Sagittalorgan" der Wirbeltiere. Z. Anat. Entwicklungsgesch. 60, 652–717.
- Agduhr, E. (1922). Über ein zentrales Sinnesorgan (?) bei den Vertebraten.
 Anat. Entwicklungsgesch. 66, 223–360.
- Vígh, B., Manzano e Silva, M.J., Frank, C.L., Vincze, C., Czirok, S.J., Szabó, A., Lukáts, A., and Szél, A. (2004). The system of cerebrospinal fluid-contacting neurons. Its supposed role in the nonsynaptic signal transmission of the brain. Histol. Histopathol. 19, 607–628.
- Stoeckel, M.-E., Uhl-Bronner, S., Hugel, S., Veinante, P., Klein, M.-J., Mutterer, J., Freund-Mercier, M.-J., and Schlichter, R. (2003). Cerebrospinal fluid-contacting neurons in the rat spinal cord, a gammaaminobutyric acidergic system expressing the P2X2 subunit of purinergic receptors, PSA-NCAM, and GAP-43 immunoreactivities: light and electron microscopic study. J. Comp. Neurol. 457, 159–174.

- Orts-Del'Immagine, A., Seddik, R., Tell, F., Airault, C., Er-Raoui, G., Najimi, M., Trouslard, J., and Wanaverbecq, N. (2016). A single polycystic kidney disease 2-like 1 channel opening acts as a spike generator in cerebrospinal fluid-contacting neurons of adult mouse brainstem. Neuropharmacology 101, 549–565.
- Djenoune, L., Khabou, H., Joubert, F., Quan, F.B., Nunes Figueiredo, S., Bodineau, L., Del Bene, F., Burcklé, C., Tostivint, H., and Wyart, C. (2014). Investigation of spinal cerebrospinal fluid-contacting neurons expressing PKD2L1: evidence for a conserved system from fish to primates. Front. Neuroanat. 8. 26.
- Fidelin, K., Djenoune, L., Stokes, C., Prendergast, A., Gomez, J., Baradel, A., Del Bene, F., and Wyart, C. (2015). State-dependent modulation of locomotion by GABAergic spinal sensory neurons. Curr. Biol. 25, 3035– 3047.
- Hubbard, J.M., Böhm, U.L., Prendergast, A., Tseng, P.-E.B., Newman, M., Stokes, C., and Wyart, C. (2016). Intraspinal sensory neurons provide powerful inhibition to motor circuits ensuring postural control during locomotion. Curr. Biol. 26, 2841–2853.
- Böhm, U.L., Prendergast, A., Djenoune, L., Figueiredo, S.N., Gomez, J., Stokes, C., Kaiser, S., Suster, M., Kawakami, K., Charpentier, M., et al. (2016). CSF-contacting neurons regulate locomotion by relaying mechanical stimuli to spinal circuits. Nat. Commun. 7, 10866.
- Jalalvand, E., Robertson, B., Wallén, P., and Grillner, S. (2016). Ciliated neurons lining the central canal sense both fluid movement and pH through ASIC3. Nat. Commun. 7, 10002.
- Jalalvand, E., Robertson, B., Tostivint, H., Wallén, P., and Grillner, S. (2016). The spinal cord has an intrinsic system for the control of pH. Curr. Biol. 26, 1346–1351.
- Sternberg, J.R., Prendergast, A.E., Brosse, L., Cantaut-Belarif, Y., Thouvenin, O., Orts-Del'Immagine, A., Castillo, L., Djenoune, L., Kurisu, S., McDearmid, J.R., et al. (2018). Pkd2l1 is required for mechanoception in cerebrospinal fluid-contacting neurons and maintenance of spine curvature. Nat. Commun. 9, 3804.
- Orts-Del'Immagine, A., and Wyart, C. (2017). Cerebrospinal-fluid-contacting neurons. Curr. Biol. 27, R1198–R1200.
- Grillner, S., and Jessell, T.M. (2009). Measured motion: searching for simplicity in spinal locomotor networks. Curr. Opin. Neurobiol. 19, 572–586.
- Ye, W., Chang, R.B., Bushman, J.D., Tu, Y.-H., Mulhall, E.M., Wilson, C.E., Cooper, A.J., Chick, W.S., Hill-Eubanks, D.C., Nelson, M.T., et al. (2015). The K + channel K IR 2.1 functions in tandem with proton influx to mediate sour taste transduction. Proc. Natl. Acad. Sci. USA 113, E229–E238.
- Li, Y., Stam, F.J., Aimone, J.B., Goulding, M., Callaway, E.M., and Gage, F.H. (2013). Molecular layer perforant path-associated cells contribute to feed-forward inhibition in the adult dentate gyrus. Proc. Natl. Acad. Sci. USA 110, 9106–9111.
- Daigle, T.L., Madisen, L., Hage, T.A., Valley, M.T., Knoblich, U., Larsen, R.S., Takeno, M.M., Huang, L., Gu, H., Larsen, R., et al. (2018). A suite of transgenic driver and reporter mouse lines with enhanced brain-celltype targeting and functionality. Cell 174, 465.e22. 480.e22.
- Dasen, J.S., and Jessell, T.M. (2009). Chapter six hox networks and the origins of motor neuron diversity. In Current Topics in Developmental Biology (Elsevier Inc.), pp. 169–200.
- Zagoraiou, L., Akay, T., Martin, J.F., Brownstone, R.M., Jessell, T.M., and Miles, G.B. (2009). A cluster of cholinergic premotor interneurons modulates mouse locomotor activity. Neuron 64, 645–662.
- Pillai, A., Mansouri, A., Behringer, R., Westphal, H., and Goulding, M. (2007). Lhx1 and Lhx5 maintain the inhibitory-neurotransmitter status of interneurons in the dorsal spinal cord. Development 134, 357–366.
- Al-Mosawie, A., Wilson, J.M., and Brownstone, R.M. (2007).
 Heterogeneity of V2-derived interneurons in the adult mouse spinal cord. Eur. J. Neurosci. 26, 3003–3015.
- 25. Bikoff, J.B., Gabitto, M.I., Rivard, A.F., Drobac, E., Machado, T.A., Miri, A., Brenner-Morton, S., Famojure, E., Diaz, C., Alvarez, F.J., et al. (2016).

Article



- Spinal inhibitory interneuron diversity delineates variant motor microcircuits. Cell 165, 207-219.
- 26. Morikawa, Y., Hisaoka, T., and Senba, E. (2009). Characterization of Foxp2-expressing cells in the developing spinal cord. Neuroscience 162, 1150-1162.
- 27. Madisen, L., Mao, T., Koch, H., Zhuo, J.M., Berenyi, A., Fujisawa, S., Hsu, Y.W.A., Garcia, A.J., Gu, X., Zanella, S., et al. (2012). A toolbox of Credependent optogenetic transgenic mice for light-induced activation and silencing. Nat. Neurosci. 15, 793-802.
- 28. Petreanu, L., Huber, D., Sobczyk, A., and Svoboda, K. (2007). Channelrhodopsin-2-assisted circuit mapping of long-range callosal projections. Nat. Neurosci. 10, 663-668.
- 29. Wickersham, I.R., Lyon, D.C., Barnard, R.J.O.O., Mori, T., Finke, S., Conzelmann, K.-K.K., Young, J.A.T.T., and Callaway, E.M. (2007). Monosynaptic restriction of transsynaptic tracing from single, genetically targeted neurons. Neuron 53, 639-647.
- 30. Lavin, T.K., Jin, L., Lea, N.E., and Wickersham, I.R. (2020). Monosynaptic tracing success depends critically on helper virus concentrations. Front. Synaptic Neurosci. 12, 6.
- 31. Djenoune, L., Desban, L., Gomez, J., Sternberg, J.R., Prendergast, A., Langui, D., Quan, F.B., Marnas, H., Auer, T.O., Rio, J.-P.P., et al. (2017). The dual developmental origin of spinal cerebrospinal fluid-contacting neurons gives rise to distinct functional subtypes. Sci. Rep. 7, 719.
- 32. Jurčić, N., Michelle, C., Trouslard, J., Wanaverbecq, N., and Kastner, A. (2021). Evidence for PKD2L1-positive neurons distant from the central canal in the ventromedial spinal cord and medulla of the adult mouse. Eur. J. Neurosci. 54, 4781-4803.
- 33. Buch, T., Heppner, F.L., Tertilt, C., Heinen, T.J., Kremer, M., Wunderlich, F.T., Jung, S., and Waisman, A. (2005). A Cre-inducible diphtheria toxin receptor mediates cell lineage ablation after toxin administration. Nat. Methods 2, 419-426.
- 34. Mendes, C.S., Bartos, I., Márka, Z., Akay, T., Márka, S., and Mann, R.S. (2015). Quantification of gait parameters in freely walking rodents. BMC Biol. 13, 50.
- 35. Gruner, J.A., and Altman, J. (1980). Swimming in the rat: analysis of locomotor performance in comparison to stepping. Exp. Brain Res. 40, 374-382
- 36. Pocratsky, A.M., Shepard, C.T., Morehouse, J.R., Burke, D.A., Riegler, A.S., Hardin, J.T., Beare, J.E., Hainline, C., States, G.J., Brown, B.L., et al. (2020). Long ascending propriospinal neurons provide flexible, context-specific control of interlimb coordination. eLife 9, 1-24.
- 37. Akay, T., and Murray, A.J. (2021). Relative contribution of proprioceptive and vestibular sensory systems to locomotion: opportunities for discovery in the age of molecular science. Int. J. Mol. Sci. 22, 1-18.
- 38. Horio, N., Yoshida, R., Yasumatsu, K., Yanagawa, Y., Ishimaru, Y., Matsunami, H., and Ninomiya, Y. (2011). Sour taste responses in mice lacking PKD channels. PLoS One 6, e20007.

- 39. Pazour, G.J., Dickert, B.L., Vucica, Y., Seeley, E.S., Rosenbaum, J.L., Witman, G.B., and Cole, D.G. (2000). Chlamydomonas IFT 88 and its mouse homologue, polycystic kidney disease gene Tg 737, are required for assembly of cilia and flagella. J. Cell Biol. 151, 709-718.
- 40. Haycraft, C.J., Zhang, Q., Song, B., Jackson, W.S., Detloff, P.J., Serra, R., and Yoder, B.K. (2007). Intraflagellar transport is essential for endochondral bone formation. Development 134, 307-316.
- 41. Orts-Del'Immagine, A., Cantaut-Belarif, Y., Thouvenin, O., Roussel, J., Baskaran, A., Langui, D., Koëth, F., Bivas, P., Lejeune, F.-X.X., Bardet, P.-L.L., et al. (2020). Sensory neurons contacting the cerebrospinal fluid require the reissner fiber to detect spinal curvature in vivo. Curr. Biol. 30, 827.e4. 839.e4.
- 42. Grillner, S., and El Manira, A. (2020). Current principles of motor control, with special reference to vertebrate locomotion. Physiol. Rev. 100,
- 43. Rudomin, P., and Schmidt, R.F. (1999). Presynaptic inhibition in the vertebrate spinal cord revisited. Exp. Brain Res. 129, 1-37.
- 44. Wu, M.-Y., Carbo-Tano, M., Mirat, O., Lejeune, F.-X., Roussel, J., Quan, F.B., Fidelin, K., and Wyart, C. (2021). Spinal sensory neurons project onto the hindbrain to stabilize posture and enhance locomotor speed. Curr. Biol. 31, 3315.e5. 3329.e5.
- 45. Madisen, L., Zwingman, T.A., Sunkin, S.M., Oh, S.W., Zariwala, H.A., Gu, H., Ng, L.L., Palmiter, R.D., Hawrylycz, M.J., Jones, A.R., et al. (2010). A robust and high-throughput Cre reporting and characterization system for the whole mouse brain. Nat. Neurosci. 13, 133-140.
- 46. Mathis, A., Mamidanna, P., Cury, K.M., Abe, T., Murthy, V.N., Mathis, M.W., and Bethge, M. (2018). DeepLabCut: markerless pose estimation of user-defined body parts with deep learning. Nat. Neurosci. 21, 1281-
- 47. Skarlatou, S., Hérent, C., Toscano, E., Mendes, C.S., Bouvier, J., and Zampieri, N. (2020). Afadin signaling at the spinal neuroepithelium regulates central canal formation and gait selection. Cell Rep. 31, 107741.
- 48. Zampieri, N., Jessell, T.M., and Murray, A.J. (2014). Mapping sensory circuits by anterograde transsynaptic transfer of recombinant rabies virus. Neuron 81, 766-778.
- 49. Dewitz, C., Pimpinella, S., Hackel, P., Akalin, A., Jessell, T.M., and Zampieri, N. (2018). Nuclear organization in the spinal cord depends on motor neuron lamination orchestrated by Catenin and Afadin function. Cell Rep. 22, 1681-1694.
- 50. R Core Team (2012). R: A language and environment for statistical computing (R Foundation for Statistical Computing). http://www. R-project.org/.
- 51. Susaki, E.A., Tainaka, K., Perrin, D., Yukinaga, H., Kuno, A., and Ueda, H.R. (2015). Advanced CUBIC protocols for whole-brain and wholebody clearing and imaging. Nat. Protoc. 10, 1709–1727.





STAR***METHODS**

KEY RESOURCES TABLE

REAGENT or RESOURCE	SOURCE	IDENTIFIER
Antibodies		
chicken anti-GFP	Abcam	RRID:AB_300798
goat anti-ChAT	Millipore	RRID:AB_90650
goat-anti FoxP2	Abcam	RRID:AB_941649
mouse-anti acetylated Tubulin	Sigma	RRID:AB_609894
rabbit anti-Calbindin	Swant	D28-K
rabbit anti-dsRed	TaKaRa	RRID:AB_10013483
rabbit anti-Lhx1	Generated in the Jessell laboratory	RRID: AB_2827967
rabbit anti-Pkd2l1	Millipore	RRID:AB_571091
sheep anti-Chx10	Abcam	RRID:AB_302278
RNAscope probes		
Mm-Slc32a1-C2	ACD	319191-C2
Mm-Slc17a6-C3	ACD	319171-C3
Bacterial and Virus Strains		
AAV-TREtight-mTag BFP2-B19G	Viral Core Facility, Charite University Berlin	N/A
AAV-FLEX-splitTVA-EGFP-tTA	Viral Core Facility, Charite University Berlin	N/A
AAV-FLEX-TVAmCherry	Viral Core Facility, Charite University Berlin	N/A
RV∆G-mCherry/EnvA	Viral Core Facility, Charite University Berlin	N/A
RVΔG-GFP/EnvA	Viral Core Facility, Charite University Berlin	N/A
Experimental Models: Organisms/Strains		
Pkd2I1-IRES-Cre	Ye et al. ¹⁸	MGI:6451758
RosaФtdTomato (Ai14)	Madisen et al. ⁴⁵	MGI:3809524
Rosa <i>Фsynaptophysin-tdTomato (Ai34)</i>	Daigle et al. ²⁰	MGI:4947243
Rosa⊅HTB	Li et al. ¹⁹	MGI:5518925
Rosa⊕ChR2 (Ai32)	Madisen et al. ²⁷	MGI:5013789
Rosa <i></i> ФDTR	Buch et al. ³³	MGI:3772576
Ift88 ^{fl}	Haycraft et al. 40	MGI:3710185
Pkd2l1 -/-	Horio et al. ³⁸	MGI:5008611
Software and Algorithms		
MouseWalker	Mendes et al. ³⁴	N/A
R	R Development Core Team	RRID: SCR_000432
Deeplabcut	Mathis et al. ⁴⁶	https://github.com/AlexEMG/DeepLab
Arivis Vision 4D	Arivis AG	N/A
Imaris	Oxford Instruments	N/A

RESOURCE AVAILABILITY

Lead contact

Further information and requests for resources and reagents should be directed to the lead contact, Niccolò Zampieri (niccolo. zampieri@mdc-berlin.de).

Material availability

All unique reagents generated in this study are available from the lead contact without restriction.

Data and code availability

- This study did not generate any unique dataset or code.
- e1 Current Biology 32, 2442–2453.e1–e4, June 6, 2022

Article



- Original data supporting the current study are available from the lead contact upon request.
- All additional information required to reanalyze the data reported in this paper is available from the corresponding lead contact
 upon request.

EXPERIMENTAL MODEL AND SUBJECT DETAILS

Animal Experimentation Ethical Approval

All animal procedures were performed in accordance to European community Research Council Directives and were approved by the Regional Office for Health and Social Affaires Berlin (LAGeSo) under license number G148/17 and the French "Direction Départementale de la Protection des Populations des Bouches-du-Rhône" (Project License Nr: APAFIS 17596; 2018111919329153. N.W. and License for the Use of Transgenic Animal Models Nr: DUO-5214).

Animal models

Mice were bred and maintained under standard conditions on a 12h light/dark cycle with access to food and water ad libitum. The day of birth was considered as postnatal day 1 (P1).

METHODS DETAILS

Ablation of CSF-cNs

To specifically ablate CSF-cNs *in vivo*, diphtheria toxin (DT; Sigma D0564) was administered intraperitoneally (50 mg.Kg⁻¹) at P40. Ablation efficiency was verified by staining for Pkd2l1.

Behavioral experiments

Mice were placed in the behavior room 30 min before starting the experiments, allowing them to acclimatize. Both sexes were included and for each test at least two representative videos with continuous movements were analyzed. For the open field test we used the ActiMot Infrared light beam activity monitor (TSE Systems). Two light-beam frames allowed to monitor X, Y and Z coordinates of the mouse. Animals were placed in the associated squared acrylic glass boxes (40 cm X 20 cm) and after 10 min of habituation time, spontaneous movements were monitored for 90 min. Data were evaluated with TSE supplied software. Gait analysis was performed as previously described. 47 Briefly, mice were placed on a customized acrylic glass walkway with surrounded LED lights to generate the internal reflection effect. A mirror under the walkway allows tracking of footprints and body outline with a high-speed camera (shutter speed 5,56 ms, frame rate 150 f/sec). Representative videos with straight and continuous runs were analyzed using the open-source MouseWalker software. To evaluate balance, we used a customized balance beam with replaceable beams of different sizes. Animals were placed on one end and had to pass the beam spontaneously to reach a shelter on the other side. A mirror was placed underneath and a high-speed camera captured the passage. The horizontal ladder was customized with side walls made of acrylic glass to create a walking path and inserted metal rungs with 3 mm diameter. Rungs had a minimum distance of 1 cm and spacing of the rungs were modified by removing individual rungs. A mirror under the horizontal ladder and the clear walls allowed tracking from the side and underneath with a high-speed camera. Animals were required to pass the walking floor spontaneously and videos with continuous runs were analyzed. For the swim task, a custom-build acrylic glass tank (10 cm X 70 cm) filled with ambient temperature water was used. Mice had to swim through the tank to reach a platform on the other end. A mirror underneath allowed monitoring swim movements with a high-speed camera. The angle between body axis and water line was obtained by using the open-source program DeepLabCut. 46 The algorithm was trained to extract coordinates of nose and tail base in all frames. A value of likelihood allowed to estimate the reliability of detected coordinates and only frames with a likelihood superior to 0.9 were used for further analysis. The x/z coordinates of indicated points allowed the calculation of the swim angle between waterline and body axis.

Perfusion and tissue preparation

Anesthesia was induced by the intraperitoneal injection of ketamine (120 mg/kg) and Xylazine (10 mg/kg). After testing the toe-pinch reflex, animals were intracardially perfused with 10 ml ice-cold PBS, followed by the perfusion of ice-cold 4 % PFA (pH 7.4). The spinal cords were exposed via laminectomy and post-fixed overnight in 4 % PFA (pH 7.4) at 4 °C. After washing for 5 min in PBS, tissue was incubated in 30% sucrose over night at 4 °C for cryoprotection. Samples were embedded in Optimal Cutting Temperature (O.C.T., Tissue-Tek) compound, frozen on dry ice and stored at -80 °C.

Slice preparation, electrophysiology and optogenetic stimulation

Pkd2l1::Cre; Rosa-Φ-ChR2(Ai32) or Pkd2l1::Cre; Rosa-Φ-ChR2(Ai32); Rosa-Φ- Rosa-Φ-tdTomato(Ai14) mice (2-4 week-old) were anesthetized with an intraperitoneal injection of a Ketamine/xylazine mixture (120/10 mg.Kg-¹) and perfused intracardiacally (>3-week-old) with an ice cold and oxygenated (95% O₂/5% CO₂) modified artificial cerebrospinal fluid (aCSF, in mM: NaCl 75, NaH₂PO₄ 1.25, NaHCO₃ 33, KCl 3, MgSO₄ 7, sucrose 58, glucose 15, ascorbic acid 2, myo-inositol 3, sodium pyruvate 2, CaCl₂ 0.5, pH 7.4, 310 mosmol.Kg⁻¹). Following laminectomy and spinal cord extraction, lumbar spinal cord coronal slices (250 to 300 μm) were prepared, transferred in a submerged incubation chamber filled with oxygenated aCSF (in mM: NaCl 115, NaH₂PO₄





1.25, NaHCO₃ 26, KCl 3, MgSO₄ 2, glucose 15, ascorbic acid 2, myo-inositol 3, sodium pyruvate 2, CaCl₂ 2; pH 7.4, 300 mosmol.Kg-1) at 35° C for 15 min and subsequently at room temperature (20-25°C) until use. For recording, slices were transferred in the perfusion chamber (aCSF 2-4 mL.min⁻¹, 20-25°C) under an epifluorescence upright microscope equipped with a CCD camera (HQ2 CoolSnap, Photometrics). Electrodes (3-6 M Ω , borosilicate glass, Harvard Apparatus) were filled with a solution containing (in mM): K-gluconate 120, NaCl 5, HEPES 10, MgCl₂ 1, CaCl₂ 0.25, EGTA 2, Mg-ATP 4, Na₂-phosphocreatine 10, Na₃-GTP 0.2 (pH 7.3, 295 mosmol.kg-1 and a chloride equilibrium potential (E_{Cl}) set at -60 mV) and 20 μM AlexaFluor488 (Invitrogen). Neurons were identified in slices under infra-red DIC illumination (IR-DIC) and recorded in whole-cell patch-clamp configuration performed in voltage- (VC) and current-clamp (CC) modes using a MultiClamp 700B amplifier (Molecular Device Inc.). Data were filtered at 2-2.4 kHz and digitized at 10 kHz using a Digidata 1322A interface driven by pClamp 9.2 (Molecular Device Inc.). Neuron intrinsic and firing properties were determined using -10 mV voltage steps (V_{Step}) from a holding potential (V_h) of -70 mV (VC) or current injection pulses (CC) from the resting membrane potential (RMP). Validation of the optogenetic approach was performed by recording Channelrhodopsin-2 (ChR2) expressing CSF-cN in VC or CC mode and ChR2 activation elicited using light pulses delivered through the objective (60x, NA 0.9; pUltra 300 CoolLED: 490 nm, with controlled power and duration). CSF-cN were recorded either in VC mode (V_h -70 mV) to characterize ChR2 photocurrent properties and voltage-dependance (V_{Step} from -90 to +10 mV, 200 ms at V_b -70 mV) or in CC mode at RMP to assess light-triggered action potentials (APs) firing. Synaptic currents were photo-evoked in CSF-cN and interneurons with 10 ms light pulses in control and in the presence of 1 µM strychnine (Sigma-Aldrich), 20 µM DNQX either alone or with 10 μM gabazine and 100 μM picrotoxin (Gbz and Ptx, BioTechne, UK). In all recordings, the liquid junction potential was left uncorrected.

Immunohistochemistry

For histology, spinal cords were with a cryostat (Leica) collected on Superfrost Plus® microscope slides (Thermo Fisher Scientific). Primary and secondary antibodies were diluted in 4 % BSA in 0.3 % TritonX in PBS. Slides were mounted with Vectashield (Vector). The following primary antibodies dilutions have been used: chicken anti-GFP (1/1000, Abcam), goat anti-ChAT (1/200; Millipore), goat-anti FoxP2 (1/200, Abcam), mouse anti-acetylated Tubulin (1/500, Sigma), rabbit anti-Calbindin (1/500, Swant), rabbit anti-dsRed (1/1000; TaKaRa), rabbit anti-Lhx1(1/10000), generated in the Jessell laboratory), rabbit anti-Pkd21I1 (1/200; Millipore), sheep anti-Chx10 (1/100, Abcam). Images were taken with a Zeiss LSM800 confocal laser scanning microscope.

Viral tracings

Intraspinal injections were performed as previously described. For analgesia, mice were subcutaneously injected with 5 mg.Kg⁻¹ Carprofen 30 min before surgery. Anesthesia was induced with continuous inhalation of isoflurane (2-3 %) in oxygen (1.5 %), using an isoflurane vaporizer (Parkland Scientific). Dorsal laminectomy was performed to expose the lumbar spinal cord prior to virus injection using a pulled borosilicate glass pipette (World Precision Instruments, Inc.) and a micro syringe pump injector (Smart Touch). For AAV, either a cocktail of AAV-TREtight-mTag BFP2-B19G (4.48*10¹² VG/mL) and AAV-FLEX-SPLIT TVA-EGFP-tTA (5.79*10¹⁰ VG/mL) was injected. A total amount of 300 nl of virus was inoculated into two adjacent spots bilaterally 40 μm left and right to the midline. After three weeks we performed intraspinal injection of 300 nl RVΔG(EnvA)-mCherry (1.94*10⁸ IU/mL) at the same position and animals were sacrificed seven days after. To analyze directionality of CSF-cN projections, we injected AAV-FLEX-TVAmCherry (5.33*10¹³ VG/mL) at L1, followed three weeks later by injection of RVΔG-GFP/EnvA (2.13*10⁸ IU/mL) either more caudally or rostrally. Mice which postmortem revealed low viral labeling or a spread into the central canal were excluded from analysis.

Fluorescent in situ hybridization

For mRNA detection via multiplex RNAscope, a modified protocol from Advanced Cell Diagnostics (ACD, 322360-USM) was used. Briefly, fixed spinal cord tissue was prepared and sectioned as described before. Spinal sections were post-fixed in 4 % PFA (pH 7.4) at 4 °C for 15 min. After washing and dehydration (at 4 °C in 50%, 70% and 100% Ethanol), a hydrophobic barrier was created around sections. After incubation with 3 % hydrogen peroxide solution (H_2O_2) at RT for 15 min, Protease IV treatment followed for 30 min at RT. C2 and C3 probes were dilutes 1/50 in sample diluent and hybridized for 2 hours at 40°C in a humid chamber in a HybEZ oven. For signal amplification and detection, the RNAscope 2.5 HD Reagents Detection Kit-RED (ACD, 32360) was used according to the manufacturer's instructions. After Detection of each channel, immunostaining was performed as described before and slices were mounted with ProLong Gold.

Positional analysis

Three-dimensional positional analysis was performed as previously described.⁴⁹ Spinal cords were sectioned in 40 µm slices and cartesian coordinates of spinal neurons per section were obtained using the imaging software IMARIS. Data were normalized to account for differences in spinal cord size and shape. The position of each neuron was digitally reconstructed by plotting the data in 'R',⁵⁰ using a customized script. Correlation analysis have been done using the "corrplot" package to calculates the comparability of experiments using the Pearson correlation coefficient. Datasets were clustered hierarchically.

Electron microscopy

Mice were perfused with 4 % (w/v) paraformaldehyde in 0.1 M phosphate buffer. Spinal cord was dissected and 2-3 mm³ cubes were fixed by immersion in 4 % (w/v) paraformaldehyde and 2.5% (v/v) glutaraldehyde in 0.1 M phosphate buffer for 2 hours at room

Current BiologyArticle



temperature (RT). Samples were postfixed with 1% (v/v) osmium tetroxide for 3 hours at RT, dehydrated in a graded series of ethanol, and embedded in PolyBed® 812 resin (Polysciences, Germany). Ultrathin sections (60-80 nm) were stained with uranyl acetate and lead citrate, and examined at 80 kV with a Zeiss EM 910 electron microscope. Acquisition was done with a Quemesa CCD camera using iTEM software (Emsis GmbH, Germany).

Tissue clearing and light-sheet microscopy

Mice were anesthetized and transcardially perfused as described above. Spinal cord was extracted after ventral laminectomy and fixed in 4% PFA for 2 days at 4°C. Tissue clearing was performed as previously described with modifications. In short, tissue was transferred to CUBIC1 (25 wt% Urea, 25 wt% N,N,N',N'-tetrakis(2-hydroxypropyl) ethylenediamine, 15 wt% Triton X-100) and incubated at 37°C shaking. Every other day CUBIC1 solution was exchanged until tissue appeared transparent (~ 4 days). Afterwards, samples were washed for 1 day with PBS at RT, refractive index matched with EasyIndex (LifeCanvas Technologies) at 37°C and imaged with the ZEISS Light-sheet Z.1. For image analysis and video rendering Arivis Vision 4D (Arivis AG) and Imaris (Oxford Instruments) was used.

QUANTIFICATION AND STATISTICAL ANALYSIS

For behavior experiments, mice were randomly allocated into different experimental groups and data have been randomized before analysis whenever possible. Quantifications represent the average of at least three biological replicates per condition. Each dot represents one animal and error bars in all figures represent mean \pm SEM. For electrophysiological experiments, data are presented as mean \pm standard deviation (SD) and graphs represent box-whisker plot using Tukey's method where single dots represent outliers. Because the data are not normally distributed (Shapiro-Wilk test), statistical significance was tested using non-parametric statistical tests: Wilcoxon signed-rank (comparison of two conditions within a group) or Kruskal-Wallis (χ^2 , degree of freedom (df) and p-value, multiple comparisons, with a post-hoc pairwise comparisons using Wilcoxon rank sum test) tests. Number of samples (n) and the applied statistical test used for individual experiments are indicated in the figure legends. Significance was defined as * p<0.05; *** p<0.01; **** p<0.001. Statistical analyses were performed using Microsoft Excel, GraphPad Prism and RStudio statistics (Version 8, GraphPad Software, RStudio v1.1.456).